Iraqi Journal of Biotechnology, 2026, Vol. 25, No. 2, 242-258

Antibacterial and Antibiofilm Activity of Nanocomposites in Multi-Drug Resistant *Streptococcus mutans*

[1]Nisreen Abbas Jdayea, Entisar E. AL- Abodi

[1]Department of Chemistry, College of Education for Pure Science- Ibn Al- Haitham, University of Baghdad, Baghdad, Iraq.

Abstract

Background. The nano-method has been used to create new, non-traditional antimicrobial agents. It is a successful treatment for infectious diseases and offers several benefits over conventional antibiotics, such as no side effects, enhanced effectiveness against drug-resistant organisms, and the ability to prevent the emergence of resistance that disrupts several biological processes. **Aim.** This study aimed to synthesize and characterize nanoparticles and investigate their antibacterial and anti-biofilm effects against *Streptococcus mutans*. **Methods.** Chitosan nanoparticles (Ch-NPs) were acquired from the Ministry of Science and Technology. FTIR analysis was used to validate the diagnosis, and a methanolic extract of *Annona muricata* was used to prepare green silver nanoparticles (Ag-NPs), which were characterized using UV-VIS spectroscopy, where the absorption of the formed AgNPs was at 427 nm at room temperature. The magnetic graphene nanocomposite (rGO/Fe3O4-NPs) was prepared physically. The nanocomposite rGO/Fe3O4.Ch-Ag-NPs was then created by combining nanoparticles of Ch-NPs, Ag-NPs, and rGO/Fe3O4-NPs (mix), and identified using scanning electron microscopy (SEM) and Fourier transform infrared spectroscopy (FTIR). Numerous tests were carried out on the nanoparticles, including assessment of antibacterial efficacy, determination of the minimum inhibitory concentration (MIC), and evaluation of biofilm development. According to the diagnostic findings, the single or mixed nanoparticles had a spherical form. Two *Streptococcus mutans* isolates were examined for antibiotic sensitivity, and the findings indicated that the isolates were resistant to the majority of drugs. **Results.** The results of the disc diffusion method evaluation of the antibacterial activity of nanoparticles revealed that, at concentrations of 128 µg/ml, the nanocomposite rGO/Fe3O4.Ch-Ag-NPs (Mix) was more effective than Ch-NPs, Ag-NPs, and rGO/Fe3O4-NPs. The *Streptococcus mutans* isolates had the highest inhibition zones, measuring 17.67 ± 0.58 and 17.33 ± 0.58 mm in isolates No. (2) and (1), respectively, when compared with Ch-NPs, Ag-NPs, and rGO/Fe3O4-NPs. Ag-NPs and Ch-NPs had a minimum inhibitory concentration (MIC) of 32 µg/ml on two *Streptococcus mutans* isolates. However, for two isolates of *Streptococcus mutans*, the MIC of the rGO/Fe3O4-NPs (Mix) was 16 µg/ml. On two isolates of *Streptococcus mutans*, however, the MIC of the rGO/Fe3O4.Ch-Ag-NPs (Mix) was 8 µg/ml. Ag-NPs and rGO/Fe3O4-NPs completely prevented *Streptococcus mutans* from forming biofilms at 16 µg/ml, whereas Ch-NPs completely prevented *Streptococcus mutans* isolates from forming biofilms at 32 µg/ml. However, at 4 µg/ml, the nanocomposite rGO/Fe3O4.Ch-Ag-NPs (Mix) completely inhibited the anti-biofilm activity of *Streptococcus mutans* isolates. **Conclusion.** The synthesized nanocomposite rGO/Fe3O4.Ch-Ag-NPs exhibited superior antibacterial and antibiofilm activities against multidrug-resistant *Streptococcus mutans* compared with the individual nanoparticles. The nanocomposite showed the lowest MIC and effectively inhibited biofilm formation, indicating its potential as a promising antimicrobial agent against resistant *Streptococcus mutans* isolates.

Keywords: *Streptococcus mutans*, *Annona muricata*, nanoparticles, Chitosan, silver, magnetic graphene.

Corresponding author: (Gmil: entisar.a.1@ihcoedu.uobaghdad.edu.iq).

Introduction

The human oral cavity is home to the second most varied microbiome in the body, with approximately 700 different kinds of bacteria (1). Dental caries is one of the most common chronic illnesses in the world. Due to its cariogenic capacity for acid generation, acid tolerance, and biofilm development, *Streptococcus mutans* is thought to be the primary cause of dental caries (2). The biofilm is a self-organised matrix of extracellular polymeric substances (EPSs) that contains a diverse array of microbial species, forming a structured community(3). In addition to aiding in the formation of biofilms, EPSs also increase the biofilms' resistance to antimicrobial treatments(4). Commensal bacteria maintenance is difficult with conventional antimicrobial treatments, such as broad-spectrum antimicrobials (5). Furthermore, the development of antibiotic resistance has made it necessary to find new antibacterial drugs that prevent the creation of EPSs and target certain oral bacterial infections (6).

Nanostructured materials have been used because of their effectiveness, longevity, and efficiency. These materials are often used in biological, physical, chemical, pharmaceutical, engineering, and environmental sciences because of their higher surface area to size ratio (7). Because of their size, shape, surface charge, stability, and concentration in the growth medium, nanomaterials are considered potential alternatives to antibiotics in the treatment of bacterial infections. The antibacterial qualities of nanomaterials are significantly influenced by the surface coatings of nanoparticles (NPs) (8). Metal and metal oxide nanoparticles are classified as mono-, bi-, tri-, or quadrometallic depending on the concentration of metals. Because of their better catalytic qualities and advantageous traits over monometallic NPs, bi-, tri-, and multimetallic NPs have attracted the most attention among them (9). Two distinct kinds of metal atoms combine to form bimetallic nanoparticles (NPs), a single nanometric substance with a variety of topologies, morphologies, and characteristics (10). Bimetallic oxide nanoparticles (NPs), including NiO/MnO, MgO/ZnO, CuO/ZnO, and Fe3O4/ZnO NPs, often exhibit unique antibacterial activity due to tensile strain and metal synergism (10).

Compared to their bulk counterparts, nanoparticles offer a more favourable environment for antibacterial treatment due to their unique properties. Many inorganic and organic nanocomposites have antibacterial qualities that allow for quick and accurate germ identification. Combinatorial delivery methods, environmental flexibility, and targeted and sustained release mechanisms are all features of antibacterial nanocomposites (11).

Materials and Methods

Bacterial isolates

Two *Streptococcus mutans* isolates were acquired from the Baghdadi City Hospital and identified using molecular (PCR) and chemical testing. The VITEK-2 System was used to confirm the diagnosis. After being re-cultured on the nutrient agar medium,It was prepared by adding 0.4% agar to the nutrient broth medium prepared according to the manufacturer's instructions, then sterilized using an autoclave. A semi-solid medium was obtained, then poured into sterile test tubes. The medium was used to test the bacteria's ability to grow. The isolates were incubated aerobically for 24 hours at 37°C.

Antibiotic susceptibility test

The Kirby-Bauer method was used to test for antibiotic sensitivity to 10 different antibiotics, as reported by the WHO in 2003(12). One or two isolated colonies of bacteria from the original culture were placed in a test tube with four milliliters of regular saline. This resulted in a bacterial suspension with a moderate turbidity compared to the standard turbidity solution, which is equivalent to 1.5×10^8 CFU/ml. Using a sterile cotton swab, a portion of the bacterial suspension was evenly and gently applied to Mueller-Hinton agar medium. The combination was then let to settle for ten minutes. Then, using sterile forceps, the antimicrobial discs were forcefully pressed onto the agar to guarantee contact. The plates were then incubated at 37°C for 18 to 24 hours after being flipped over. Using a metric ruler, the inhibition zones that developed around the discs were measured in millimetres (mm) in accordance with the Clinical Laboratories Standards Institute recommendations (13).

Assessment of biofilm formation

Streptococcus mutans biofilm development was assessed using the method outlined by Patel *et al*. (14); all isolates were grown overnight at 37 °C in Brain Heart Infusion Broth. Using pipetting, each isolate was thoroughly mixed with 1% glucose-containing tryptic soy broth (TSB). The bacterial isolate's suspension was altered to meet the McFarland No. 0.5 turbidity standard.

In triplicate, 200 µl of each isolate's culture was added to a sterile, flat-bottomed 96-well microtiter plate. The plates were placed in an aerobic environment at 37°C for 24 hours after being covered with lids. To get rid of any germs that could have come loose during incubation, distilled water was used twice to rinse the planktonic cells. The bacterial cells in each well were fixed in 200 µl of 100% methanol for 20 minutes at room temperature. For 15 minutes, 200 µl of 0.1% crystal violet was added to each well in order to stain the adhering cells. Following the completion of the staining process, the excess stain was periodically washed away with distilled water two to three times. To remove the stain, 33% acetic acid was poured to the plate after it had been left at room temperature for around 30 minutes to ensure it was totally dry. The optical density (OD) at 630 nm was measured using an ELISA auto reader. Each test result was deducted from the average optical density values of the sterile medium. Additionally, the cut-off value (ODc) was calculated to determine whether or not isolates produced biofilms (15).

ODc: Average OD of negative control + (3 × standard deviation (SD) of Negative control), OD isolate: Average OD of isolate – ODc.

According to the cutoff value (ODc) calculation, the biofilm detection result is as follows:

ODc ≥ OD (no biofilms are produced), **2 × ODc ≥ OD > ODc** (biofilm production weak), **2 ×ODc < OD ≤ 4 × ODc** (moderate biofilm production), **OD > 4× ODc** (strong biofilm production).

Collection of *Annona muricata*

Annona muricata was purchased from regional Iraqi marketplaces. Following collection, the Annona fruits were cleaned with water, the outer peel was separated, and the seedless inner peel (pulp) was gathered and dried for five days at 40 degrees Celsius in an oven. It was dried and then processed into a powder with an electric grinder. A one-to-five (weight/volume) ratio was used to create the suspension. Add methanol to a beaker, shake it at 100

rpm for three hours at room temperature, filter it using filter paper, use a rotary evaporator to concentrate the filtrate, and store it at 4 degrees Celsius until it's time to utilise it.

Preparation of chitosan, silver and magnetic graphene nanoparticles and nanocomposite rGO/Fe3O4.Ch-Ag-NPs (Mix)

Chitosan nanoparticles (Ch-NPs) were obtained from the Ministry of Science and Technology, and the diagnosis was validated using FTIR analysis. Typically, dissolve 1 g of powdered chitosan in 5% acetic acid and stir for 30 minutes. To obtain a clear solution, this was then filtered. Following the addition of 2.5 mL 1 M NaOH.

The green silver nanoparticles were prepared using *Annona muricata* (AgNPs) methanolic extract, as described by Ojha *et al*. (16), with certain changes. Using an ultrasonic power of 100 W and a frequency of 42 kHz, 5 ml of each extract was sprayed dropwise into 95 ml of a 10 mM silver nitrate AgNO3 solution (prepared by dissolving 1.69 g $AgNO_3$ in 1 L deionised water) at a flow rate of 0.2 ml/min. The solutions were sonicated for 20 minutes, then stirred for 30 minutes at 800 rpm at 25°C. They were then kept in dark bottles at 25°C for 48 hours. To get a clear supernatant, the reaction mixture was centrifuged for 10 minutes at 10,000 rpm after a 24-hour period. The finished colloid samples were stored in dark jars at 4°C. The colour of solutions containing *Annona muricata* silver nanoparticles (Ag-NPs) altered from dark green to light brownish green over the course of five days; this colour shift signifies the development of Ag-NPs. Ag-NPs have been described by FTIR analysis and scanning electron microscopy (SEM).

To prepare the rGO/Fe_3O_4 nanocomposit, place 0.6 g of graphene nanopowder (GO) in a beaker with 100 ml of a previously prepared solution of hydrochloric acid (HCl) at a concentration of 0.5 M. Stir with a magnetic stirrer for 15 minutes. Add 5.6 g of anhydrous iron trichloride ($FeCl_3$) and stir for another hour. After 24 hours, leave the solution for 15 minutes. Finally, add 4.2 g of ferrous sulphate and aqueous ($FeSO_4.7H_2O$) to the resultant solution and stir for 15 minutes. A solution of sodium hydroxide (NaOH) at a concentration of 1 M is made by weighing and dissolving 5 g of sodium hydroxide in distilled water in a 125 ml volumetric flask. Then, it is added to the previous solution in the form of drops at a temperature of 80˚ C while vigorously stirring until it reaches PH = 12. We observe the formation of a black precipitate that is nano-magnetic iron oxide on the graphene oxid sheets, as it was observed to be drawn to the magnet. After repeatedly washing the precipitate with distilled water devoid of ions until the solution turned neutral, it was dried for four hours at 60˚C (17). FTIR analysis and scanning electron microscopy (SEM) have been used to characterise rGO/Fe3O4-NPs.

Chitosan nanoparticles, AgNPs, and rGO/Fe3O4 were mixed together to form the nanocomposite rGO/Fe3O4.Cs-Ag-NPs (Mix) was made by dissolving 5 ml of chitosan (Ch) in 15 ml of nanosilver extract (AgNPs) containing 10 mg of folic acid (FA) and combining it with 0.2 g of magnetic graphene iron oxide (rGO/Fe3O4) (18).

Characterization of the prepared nanoparticles

Fourier Transform Infrared (FTIR) Spectroscopy Analysis

The FTIR analysis (Shimadzu) was used to characterise the functional groups on the surface of Ch-NPs, Ag-NPs, and rGO/Fe3O4-NPs. The spectra were scanned at a resolution of 4 cm^{-1} in the 4000–400 cm^{-1} range. The samples were produced by spreading them on a glass slide in accordance with normal protocols. The sample was then examined (19).

Scanning Electron Microscopy Analysis

A Te-Scan Vega Easyprpbe (Japan) scanning electron microscope (SEM) was used to analyse the morphology of the produced nanoparticles. The morphological features of the samples were evaluated using SEM analysis. The samples were created by distributing them on a glass slide (almost seven drops on the slide) in accordance with standard procedures. A constant voltage was then applied while the sample was examined and measurements were collected at 5000x, 10000x, 20000x, and 50000x magnification (20).

Study the antibacterial activity of chitosan, silver and magnetic graphene nanoparticles and nanocomposite rGO/Fe3O4.Ch-Ag-NPs (Mix) Disc diffusion method

In accordance with Razmavar *et al*. (21) standard technique, the disc diffusion method was used to evaluate the nanoparticles' antibacterial activity. The bacterial culture (adjusted to 0.5 McFarland standard) was uniformly injected onto Muller Hinton agar plates using a sterilised brush. After drying for 15 minutes, the plates were used for the sensitivity test. This was followed by diluting the stock solution to yield concentrations of 128 µg/ml of nanoparticles. Each dilution was impregnated into 20 microlitres of sterile blank discs with a diameter of 6 mm. DMSO discs and pure water were used as negative controls. Before each disc was put on the Mueller Hinton agar surface, it had been completely dried. For a whole day, the plates were incubated at 37°C. The diameter of the inhibitory zone surrounding the discs was measured to assess the antibacterial activity following incubation. To guarantee dependability, the test was conducted three times.

Determination of Minimum Inhibitory Concentration (MIC) of nanoparticles

The MIC of the nanoparticles in a 96-well microtiter plate was ascertained using the broth microdilution technique. A concentration of 128 µg/ml of nanoparticles was produced in broth as a working solution. Immediately on the plate, consecutive two-fold dilutions of the nanoparticles were made in order to reach the concentrations of 128-1 µg/ml. 100 µl of the generated nanoparticles (ch-NPs, Ag-NPs, rGO/Fe3O4-NPs, and the nanocomposite rGO/Fe3O4.Ch-Ag-NPs (Mix)) were introduced into row A's first wells. Only 100 µl of broth was present in columns B–H. Methodical double serial dilutions were made down the columns (from rows A-H) using micropipettes. The 100 µl broth was moved to the next row and well mixed after 100 µl was taken out of the initial concentrations in row A. The final 100 µl was disposed of after repeating this procedure all the way to row (H). The final volume in each test well containing the nanoparticles is now 100 µl, except for the column, which had 200 µl of broth for sterility control. Except for the negative control, 100 µl of the 1×10^8 CFU/ml bacterial inoculum was applied to each well. Microtiter plates were incubated at 37 °C for 20 hours. Following the incubation period, 20 µl of resazurin dye was added to each well and left for 30 minutes in

order to monitor any colour changes. By determining the lowest concentrations of nanoparticles at which the colour of the resazurin broth test did not shift from blue to pink, the MIC was visually determined in broth microdilutions (22).

Study the antibiofilm activity of chitosan, silver and magnetic graphene nanoparticles and nanocomposite rGO/Fe3O4.Ch-Ag-NPs (Mix)

To ascertain the anti-biofilm activity of Ch-NPs, Ag-NPs, rGO/Fe3O4-NPs, and the nanocomposite rGO/Fe3O4.Ch-Ag-NPs (Mix), a 96-well microtiter plate was employed. The concentrations (128-1) µg/ml were achieved by preparing the nanoparticles' working solution at 128 µg/ml. In row A, 200 µl of each sample was added to the first wells. Only 100 µl of the broth was present in the columns that included rows B–H. Using a micropipette, twofold serial dilutions were methodically made down the columns (from rows A-H). After 100 µl of the broth had been taken out of the initial concentrations in row A and transferred to the following row, the procedure was repeated until the last row (H), where the final 100 µl was discarded. Except for the negative control, 100µl of the 1×10^8 CFU/ml bacterial inoculum was applied to each well. The process outlined in the paragraph (**Assessment of biofilm growth**) was followed.

Statistical Analysis

from the Statistical Analysis System SAS (23), was used to assess how various factors influenced the research parameters. In this study, the means were statistically compared using the ANOVA method of the least significant difference (LSD).

Results

Antibiotic susceptibility test

Using the CLSI (13) guidelines and the disc diffusion technique, the antibiotic susceptibility of *Streptococcus mutans* isolates was determined based on the inhibitory zone diameter (mm). In this experiment, ten antibiotics (Ceftriaxone, Amikacin, Vancomycin, Ciprofloxacin, Levfloxacin, Chloranaphenicol, Rifampin, Tobramycin, Meropenem, Methicilli,**)** were evaluated against two *Streptococcus mutans* isolates. The data revealed that *Streptococcus mutans* isolates have unusually high levels of resistance to the medications used. These two *Streptococcus mutans* isolates were found to be 50% resistant to several antibiotics, as shown in Table (1,2).

.

Table (1): Volumes and concentrations of qRT-PCR reaction mix.

Component	Volume (µl)
Luna Universal qPCR Master Mix	10
Forward primer (10 µM)	1
Reverse primer (10 µM)	1
Template DNA	5
Nuclease-free Water	3
Total	**20**

Table (2): Antibiotic susceptibility test of *Streptococcus mutans* isolates.

Isolates	CRO	AK	VA	CIP	LEV	C	RA	TOB	ME	MEM	Percentage of resistance
***Sm*1**	R	S	R	S	S	R	R	S	R	S	50%
***Sm*2**	R	S	R	S	S	R	R	S	R	S	50%

(Sm): *Streptococcus mutans,* **(CRO):** Ceftriaxone, **(AK):** Amikacin, **(VA):** Vancomycin, **(CIP):** Ciprofloxacin, **(LEV):** Levfloxacin, **(C):** Chloranaphenicol, **(RA):** Rifampin, **(TOB):** Tobramycin. **(MEM):** Meropenem, **(ME):** Methicilli,

Characterization of chitosan, silver and magnetic graphene nanoparticles

The morphological, structural, and optical properties of synthesised Ch-NPs, Ag-NPs, and rGO/Fe3O4-NPs have been assessed using the following methods:

Fourier Transform Infrared (FTIR) Spectroscopy Analysis

FTIR spectroscopy is one of the most important and widely used analytical methods for determining functional groups in synthesized nanomaterials (26).

FTIR spectra were recorded in the range of 4000 cm^{-1} to 670 cm^{-1} (2.5 μm to 15 μm), and in some cases down to 400 cm^{-1} (25 μm). The FTIR spectra revealed the presence of various functional groups associated with the synthesized nanomaterials.

The FTIR spectra of Ag-NPs showed a discernible band of absorbance at peaks (1076.28, 1382.96, 1620.21, and 3169.04) cm^{-1}. The peak at 1382.96 cm^{-1} in Ag-NPs was identical to $AgNO_3$ and absent in the plant extract, confirming the formation of Ag-NPs.

According to Das et al. (32), alterations in functional groups of active biomolecules indicate their involvement in the synthesis of Ag-NPs.

Figure (3) shows FTIR bands of chitosan nanoparticles at (3394.72, 2873.94, 1651.07, 1375.25, 1155.36, 1074.35, 994.97, 663.51, 596.00, and 422.41) cm^{-1}. The appearance of new peaks compared with chitosan indicates the formation of a new nanocomposite structure, confirming successful nanoparticle formation (33).

rGO/Fe_3O_4-NPs exhibited functional groups such as C-H stretching, N-H bending, C-C stretching, C-N stretching, and phenolic-OH stretching. The peaks appeared at (3388.93, 3066.82, 1597.06, 1340.53, 1116.78, 894.97, 794.67, 569.00, and 403.12) cm^{-1}, as shown in Figure (4).

Table (3): FTIR spectral peak values and functional groups (4000 – 400 cm^{-1}) obtained for methanol fruit pulp extract of *Annona muricata.*

No.	Peak Value	Functional groups
1	428 cm^{-1}	Alkyl halides
2	520 cm^{-1}	R-Br, C-Br Stretch
3	777 cm^{-1}	Alkyl halides
4	817 cm^{-1}	R-CL, C-CL Stretch
5	866 cm^{-1}	Aromatics 1,3, 5, trisub, C-H out of plane
6	921 cm^{-1}	Carboxylic acid RCO-OH, RCOOH O-H bend
7	1053 cm^{-1}	Alkyl halides
8	1257 cm^{-1}	Alkanes CH3
9	1421 cm^{-1}	Aromatics C-C in ring, Ar C-C Stretch
10	1620 cm^{-1}	Alkenes Ar-CH=CHR
11	1735 cm^{-1}	Alkynes RC=CH, C=C Stretch
12	2927 cm^{-1}	Alkanes RCH_2CH_3, CH Stretch
13	3375 cm^{-1}	Phenols ArO-H, H-bonded

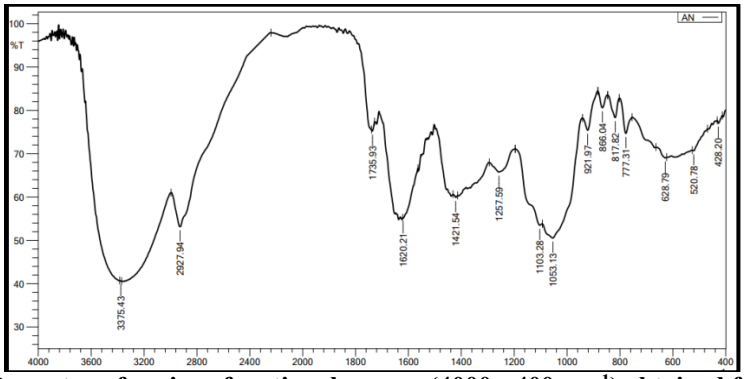

Figure (1): FT-IR spectra of various functional groups (4000 - 400 cm^{-1}) obtained for methanol fruit pulp extract of *Annona muricata*.

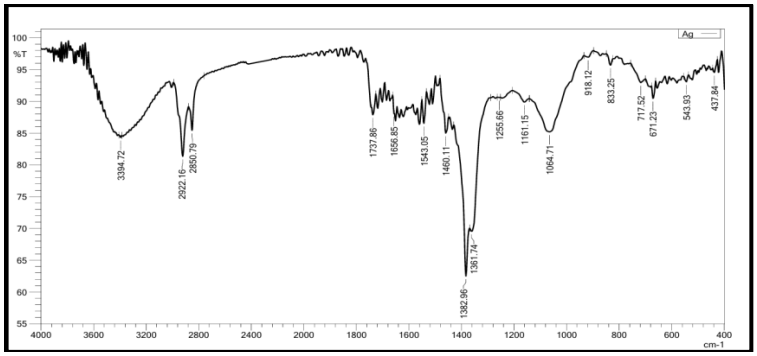

Figure (2): FTIR spectra of functional groups from the Ag-NPs.

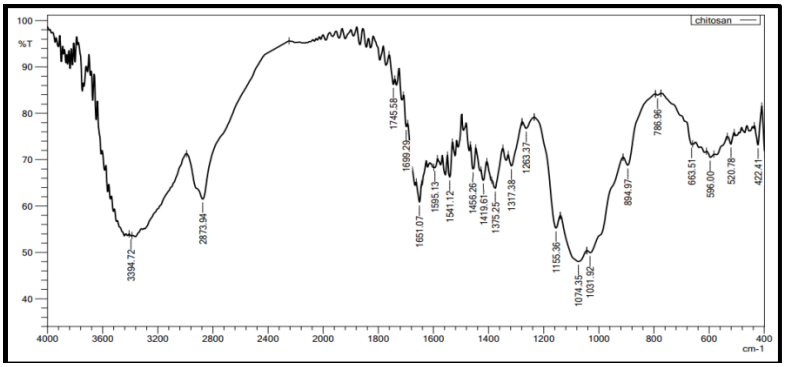

Figure (3): FTIR spectra of functional groups from the Ch-NPs.

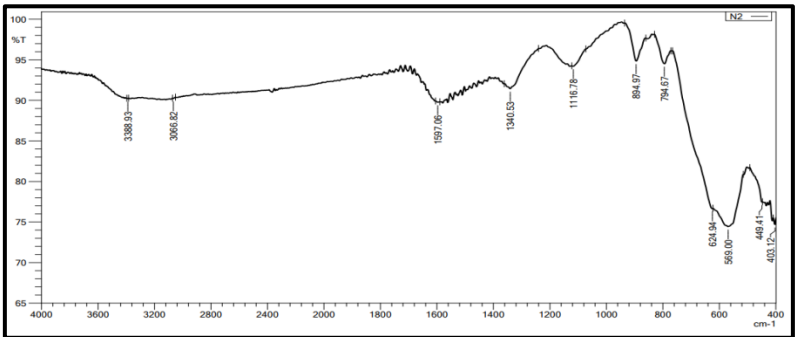

Figure (4): FTIR spectra of functional groups from the rGO/Fe3O4-NPs.

Scanning electron microscope

SEM analysis was used to investigate the morphology of synthesized nanoparticles. The results showed that Ag-NPs and rGO/Fe_3O_4-NPs were predominantly spherical and nanosized. However, aggregation of particles was observed, which may be due to biomolecular capping agents present on the nanoparticle surface (34). This aggregation acted as a stabilizing factor. These findings are consistent with previous studies, where Ag-NPs synthesized from plant extracts showed spherical and agglomerated structures (35, 36, 37).

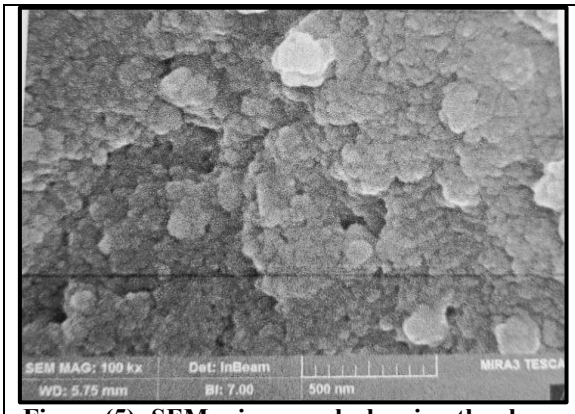

Figure (5): SEM micrograph showing the shape of AgNPs.

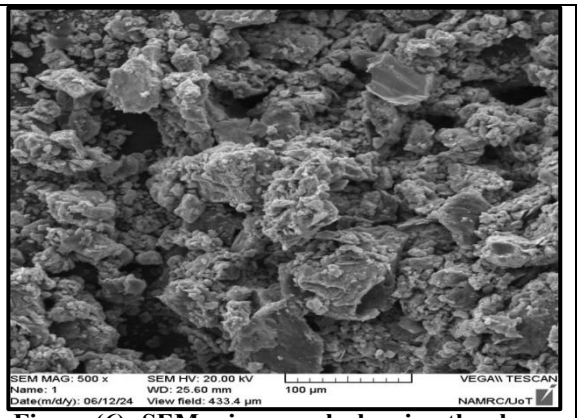

Figure (6): SEM micrograph showing the shape of rGO/Fe3O4-NPs.

Antibacterial activity of chitosan, silver and magnetic graphene nanoparticles and nanocomposite rGO/Fe3O4.Ch-Ag-NPs (Mix)

Disk diffusion method

The antibacterial activity of Ch-NPs, Ag-NPs, rGO/Fe3O4-NPs, and rGO/Fe3O4.Ch-Ag-NPs (Mix) against isolates of *Streptococcus mutans* was assessed using the disk-diffusion technique. According to the results, the nanocomposite rGO/Fe3O4.Ch-Ag-NPs (Mix) was more effective than Ch-NPs, Ag-NPs, and rGO/Fe3O4-NPs at concentrations of 128 µg/ml on *Streptococcus mutans* isolates. In isolates (No. 2 and 1), the highest inhibition zone was 117.67 ± 0.58 and 17.33 ± 0.58 mm, respectively. This difference was significant (P≤0.01), as shown in Table (3).

Table (4): Antibacterial activity of (Ch-NPs, Ag-NPs, rGO/ Fe_3O_4-NPs and rGO/Fe3O4.Ch-Ag-NPs) on *Streptococcus mutans.*

Isolate	Nanoparticles (128 µg/ml)				LSD value
	Mean ± SD				
	Ch-NPs	Ag-NPs	rGO/Fe_3O_4-NPs	rGO/Fe3O4.Ch-Ag-NPs	
***Sm*1**	13.33 ± 0.58	13.67 ± 0.58	15.33 ± 0.58	17.33 ± 0.58	1.582**
***Sm*2**	13.00 ± 1.00	13.00 ± 1.00	14.67 ± 0.58	17.67 ± 0.58	2.237**
LSD value	3.069 N.S	3.069 N.S	2.170 N.S	2.170 N.S	----
** (P≤0.01)					

(SM): ***Streptococcus mutans***

Determination of the (MIC) of the Ch-NPs, Ag-NPs, rGO/Fe3O4-NPs and rGO/Fe3O4.Ch-Ag-NPs (Mix)

The MIC of Ch-NPs, Ag-NPs, rGO/Fe_3O_4-NPs, and rGO/Fe_3O_4.Ch-Ag-NPs (Mix) was determined using a 96-well microtiter plate and broth microdilution method. The results showed that, (Ch-NPs and Ag-NPs: 32 µg/ml, rGO/Fe_3O_4-NPs: 16 µg/ml, rGO/Fe_3O_4.Ch-Ag-NPs (Mix): 8 µg/ml)

Thus, the nanocomposite showed the highest antibacterial efficiency among all tested nanoparticles.

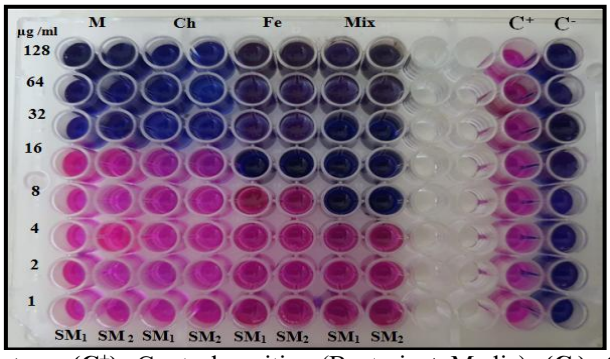

(SM): ***Streptococcus mutans***, **(C^+):** Control positive (Bacteria + Media), **(C^-):** Control negative (Media only), **(M):** Ag NPs, **(Ch):** ChNPs, **(Fe):** rGO/Fe3O4-NPs, **(Mix):** rGO/Fe3O4.Ch-Ag-NPs.

Figure (7): MIC of (Ch-NPs, Ag-NPs, rGO/Fe3O4-NPs and rGO/Fe3O4.Ch-Ag-NPs) on *Streptococcus mutans*

Table (5): MIC of (Ch-NPs, Ag-NPs, rGO/Fe3O4-NPs and rGO/Fe3O4.Ch-Ag-NPs) on *Streptococcus mutans*.

Isolate	SM_1	SM_2
	MIC (µg/ml)	MIC (µg/ml)
Ag-NPs	32	32
Ch-NPs	32	32
rGO/Fe3O4-NPs	16	16
rGO/Fe3O4.Ch-Ag-NPs (Mix)	8	8

(SM): ***Streptococcus mutans***,

Anti-Biofilm activity of chitosan, silver and magnetic graphene nanoparticles and nanocomposite rGO/Fe3O4.Ch-Ag-NPs (Mix)

Biofilm formation was evaluated using the microtiter plate method, and absorbance was measured at 630 nm using an ELISA reader.

The mean optical density of isolates was 0.435 ± 0.287, ranging from 0.215 to 0.622. All isolates showed 100% strong biofilm formation (Table 5).

Table (6): Biofilm formation of *Streptococcus mutans* isolates before and after treatment with (Ch-NPs, Ag-NPs, rGO/Fe3O4-NPs and rGO/Fe3O4.Ch-Ag-NPs)

Before treatment								
	SM_1	SM_2	SM_1	SM_2	SM_1	SM_2	SM_1	SM_2
	Strong	Strong	Strong	Strong	Strong	Strong	Strong	Strong
After treatment								
µg/ml	Ag-NPs		Ch-NPs		rGO/Fe3O4-NPs		rGO/Fe3O4.Ch-Ag-NPs	
	SM_1	SM_2	SM_1	SM_2	SM_1	SM_2	SM_1	SM_2
1	Weak	Moderate	Moderate	Strong	Moderate	Moderate	Weak	Moderate
2	Weak	Weak	Moderate	Moderate	Moderate	Weak	Weak	Weak
4	Weak	Weak	Moderate	Moderate	Weak	Weak	No Biofilm	No Biofilm
8	Weak	Weak	Weak	Moderate	Weak	Weak	No Biofilm	No Biofilm
16	No Biofilm	No Biofilm	Weak	Weak	No Biofilm	No Biofilm	No Biofilm	No Biofilm
32	No Biofilm	No Biofilm	No Biofilm	No Biofilm	No Biofilm	No Biofilm	No Biofilm	No Biofilm
64	No Biofilm	No Biofilm	No Biofilm	No Biofilm	No Biofilm	No Biofilm	No Biofilm	No Biofilm
128	No Biofilm	No Biofilm	No Biofilm	No Biofilm	No Biofilm	No Biofilm	No Biofilm	No Biofilm

(SM): *Streptococcus mutans* isolates.

Discussion

They can have this capacity spontaneously, through genetic material mutations or horizontal gene transfer (24).

Overuse of antibiotics causes microorganisms to develop resistance to various drugs. As a result, these bacteria have developed antibiotic resistance and cross-resistance, as well as multi-drug resistant MDR forms (25). The development of fresh and imaginative antimicrobial medicines is critical because to the growth of resistance isolates. As a result, scientists are always searching for new strategies to tackle microbial populations that are resistant to a wide range of medications.

FTIR spectroscopy is one of the most important and widely used analytical methods for determining if a certain functional group is present in a synthesised nanomaterial (26).

Fourier Transform Infra-Red (FTIR) spectrophotometers were used to record spectra in the 4000 cm^{-1} to 670 cm^{-1} (2.5 µm to 15 µm) range, or sometimes as low as 400 cm^{-1} (25 µm). The FTIR spectra of the methanolic extracts of *Annona muricata* showed the presence of many functional groups, such as phenolic–OH group stretching, C-H stretching, N-H bend, C-C stretching, and C-N stretching. The peaks between 4000 and 3200 cm–1 were identified as O-H stretching and aldehydic C-H stretching, respectively (27). This is equivalent to alkanes, primary amines, and carboxylic acids (28). The C–C stretching bond, shown by peak 1384 cm^{-1}, indicates the presence of aromatic compounds, whereas the N–O symmetric stretching, represented by peaks 1109 and 1055 cm^{-1}, respectively, indicates the presence of nitro compounds (29). Protein carbonyl stretching is the cause of the peak at 1641 cm^{-1} (N–H) (30). The presence of ester is shown by the tiny peaks located at about 1000 cm^{-1}. The smallest peaks, measuring 600 cm^{-1} or less, show the presence of C-Cl stretching of alkyl halides. At their maxima, there were noticeable bands of absorption. As shown in (Table 2) (Figure 1).

Furthermore, the AgNO3 FTIR spectra showed a discernible band of absorbance at peaks (1382.96) cm^{-1}(31). Additionally, the Ag-NPs methanolic extract samples showed discernible bands of absorbance at peaks (1076.28, 1382.96, 1620.21, and 3169.04) cm^{-1}, according to the FTIR spectroscopy (Figure 2). The peak (1382.96) in the Ag-NPs methanolic extracts' FTIR spectra is identical to the AgNO3 sample's peak and was absent from the *Annona muricata* methanolic extract. Thus, this signifies the development of (Ag-NPs).

According to Das *et al*. (32), alterations in the functional groups of active biomolecules may reveal their involvement in the synthesis of Ag-NPs.

Figure (3) illustrates the strong absorption bands or bands at the peaks of the chitosan nanoparticle (3394.72, 2873.94, 1651.07, 1375.25, 1155.36, 1074.35, 994.97, 663.51, 596.00, 422.41) cm^{-1}. A new spectrum that was absent from the Chitosan spectra when comparing the spectra of Chitosan nanoparticles with those of Chitosan in earlier studies emerged in the nanocomposite, signifying the formation of a new bond. These modifications to the bioactive compounds' functional groups suggest a connection to the chitosan nanoparticle production process. The changing peaks imply the development of a new compound, according to Jabbar Almukhtar and Karam's (33) supporting evidence for nanocomposite production.

Numerous functional groups, such as C-H stretching, N-H bend, C-C stretching, C-N stretching, and phenolic–OH group stretching, were seen in the rGO/Fe3O4-NPs' FTIR spectra. As seen in Figure (4), they displayed noticeable bands of absorbance at peaks (3388.93, 3066.82, 1597.06, 1340.53, 1116.78, 894.97, 794.67, 569.00, 403.12) cm^{-1}.

Scanning electron microscopy (SEM), one of the widely used techniques for characterising the synthesised nanoparticles, was employed to analyse the form and morphology of the green nanoparticles. The findings support the idea that nanoparticles come in a wide range of sizes and forms.

Using a SEM, the surface of Ag-NPs and rGO/Fe3O4-NPs has been examined. As seen in Figures 5 and 6, SEM examination revealed that the particles are spherical in form and nanometres in size for Ag-NPs and rGO/Fe3O4-NPs. Large nanoparticles were also seen as a result of aggregation. This aggregation, which serves as a capping agent, was caused by cell components on the nanoparticle surface (34).

This result was in line with Surega's (35) use of SEM to analyse the synthesised AgNPs' form using aqueous leaf extracts of *Tridax procumbens*, *Euphorbia hirta*, and *Azadirachta indica*. The findings showed that the AgNPs were agglomerated and spherical. According to a previous study, silver nanoparticles synthesised from *Crocus sativus* L extract had a spherical shape and an average particle size of 20–30 nm, as determined by SEM analysis (36).

A scanning electron microscope (SEM) image of the AgNPs produced by *Phyllanthus niruri* extraction under optimal physical conditions shows that they are about 100 nm in size and come in a number of shapes, with spherical being the most common shape and triangular, rhombus, and other shapes being detected. Additionally, SEM analysis revealed the creation of evenly distributed AgNPs and the visible aggregation of the particles (37). According to this finding, the concentration-dependent efficiency of

the Ch-NPs, Ag-NPs, rGO/Fe3O4-NPs, and rGO/Fe3O4.Ch-Ag-NPs (Mix) used in this experiment is in line with previous metal oxide nanoparticle reports from other studies(45). Furthermore, it has been noted that the antibacterial effectiveness of nanoparticles is significantly influenced by their diameters (38). Because of their many shapes, vast surface area, charge, adsorption, and chemical reactivity, they may interact with biological systems in an efficient manner and greatly hinder them (46). Consequently, the antibacterial efficacy of Ch-NPs, Ag-NPs, rGO/Fe3O4-NPs, and rGO/Fe3O4.Ch-Ag-NPs (Mix) was significantly influenced by their nanometre sizes.

The results of this study are consistent with those of Azhir *et al*.(47), who verified that the nanoparticles exhibited potent antibacterial activity against both Gramme positive and Gramme negative bacteria using the broth microdilution method. Furthermore, it was demonstrated that NPs' antimicrobial effect made *B. subtilis*, *E. coli*, and *P. aeruginosa* susceptible to them; this sensitivity grew as the concentration increased(48). The generation of biofilms was measured using the Microtiter plate technique, and the intensity of the biofilm was evaluated by measuring the absorbance at 630 nm using an ELISA reader. The isolates' mean optical density was 0.435 ± 0.287, ranging between 0.215 to 0.622. The results showed that all isolates exhibited 100% robust biofilm growth, as shown in Table 5. Ag-NPs and rGO/Fe3O4-NPs completely prevented *Streptococcus mutans* from forming biofilms at 16 µg/ml, whereas Ch-NPs completely prevented *Streptococcus mutans* isolates from forming biofilms at 32 µg/ml. However, at 4 µg/ml, the nanocomposite rGO/Fe3O4.Ch-Ag-NPs (Mix) completely suppressed the antibiofilm activity of *Streptococcus mutans* isolates.

The microtiter plate has been the most widely used and accepted test for the detection of biofilm formation because of its high throughput screening capabilities, ease of handling, and faster and more precise way of measuring the contact cell attachment and biofilm formation of different bacterial strains (49).

Bacteria and other microorganisms create complex structures known as bacterial biofilms due to their propensity to develop multidrug resistance, evade host defences, and withstand a variety of stresses. These structures are linked to chronic bacterial infections that affect humans and other organisms and represent a significant global health concern (50). Previous studies have demonstrated a connection between the multi-drug resistance phenotype of a number of bacterial species and their ability to form biofilms (51). The significance of biofilm and its part in the development of high antibiotic resistance by some bacterial species were emphasised by Mahdi and AL-Azawi (25). According to Ramos *et al*. (52), bacteria can form a biofilm to adhere to host cells.

Because of the different synergistic impacts of the separate components, nanoparticles have many functions and display increased and cumulative features. This work supports Basavegowda and Baek (43) findings that metal and metal oxide nanoparticles' antibacterial efficacies have been evaluated against a range of pathogenic strains that are both resistant to and sensitive to antibiotics. Many infectious disorders are primarily caused by pathogenic bacteria, such as *E. Coli, P. aeruginosa, S. mutans,* and *S. aureus*. These harmful bacteria

endanger human health and cause significant problems for the healthcare system.

Rajkumari *et al*. (53) state that bacterial resistance to antibiotics has been connected to the formation of biofilms. Biofilm development is inhibited by Ch-NPs, Ag-NPs, rGO/Fe3O4-NPs, and rGO/Fe3O4 treatments. rGO/Fe3O4.Ch-Ag-NPs (Mix) invade and colonise host tissue, demonstrating their pathogenicity. The observed prevention of biofilm growth is consistent with the findings of Cai *et al*. (54), who discovered a concentration-dependent link between biofilm inhibition capacity and bacterial motility (55). They can have this capacity spontaneously, through genetic material mutations or horizontal gene transfer (24).

Overuse of antibiotics causes microorganisms to develop resistance to various drugs. As a result, these bacteria have developed antibiotic resistance and cross-resistance, as well as multi-drug resistant MDR forms (25). The development of fresh and imaginative antimicrobial medicines is critical because to the growth of resistance isolates. As a result, scientists are always searching for new strategies to tackle microbial populations that are resistant to a wide range of medications.

Conclusions

According to the current study, multimetallic nanoparticles (NPs) and their composites may find use in a variety of medical applications and in the near future to produce more powerful antimicrobial agents that will prevent the emergence and spread of bacterial resistance to conventional antibiotics. It was discovered that the nanoparticles (Ch-NPs, Ag-NPs, rGO/Fe3O4, and Ch-Ag-NPs (Mix)) showed a strong anti-biofilm agent on *Streptococcus mutans* isolates, despite the fact that the bacterial isolates had produced large biofilms before treatment. Additionally, even though the bacterial isolates were resistant to widely used antibiotics, the combination of rGO/Fe3O4.Ch-Ag-NPs shown a higher level of antibacterial activity against multidrug-resistant *Streptococcus mutans* than did Ch-NPs, Ag-NPs, and rGO/Fe3O4. As a result, they can be utilised to treat infectious disorders brought on by germs that are resistant to therapy.

References

1. Pathak, J. L.; Yan, Y.; Zhang, Q.; Wang, L.; and Ge, L. (2021). The role of oral microbiome in respiratory health and diseases. Respiratory Medicine, 185, 106475.
2. Hattab N. J., Al Abodi, E. E.& Laibi, E. (2022)." Development of the Properties of Zinc Polycarboxylate Cement Used as a Basis for Dental Fillings Using Zinc Oxide Nanoparticles Prepared by Green Chemistry Method", IHJPAS. 37 (1) 202.
3. Jakubovics, N. S.; Goodman, S. D.; Mashburn-Warren, L.; Stafford, G. P. and Cieplik, F. (2021). The dental plaque biofilm matrix. *Periodontol,* 86 (1): 32–56.
4. Mohamed, I. E. and AL-Azawi, A. H. (2022). Evaluation of Antibacterial Activity of Laurus nobilis Leaves Extract against Escherichia coli Isolates, Iraqi Journal of Biotechnology, 21(2): 623-631.
5. Huang, Y.; Liu, Y.; Shah, S.; Kim, D.; Simon-Soro, A.; Ito, T., *et al*. (2021). Precision targeting of bacterial pathogen *via* bi-functional nanozyme activated by biofilm microenvironment. Biomaterials, 268: 120581–120605.
6. Xia, M. Y.; Xie, Y.; Yu, C. H.; Chen, G. Y.; Li, Y. H.; Zhang, T., *et al*. (2019). Graphene-based nanomaterials: the promising active agents for antibiotics-independent antibacterial applications. Journal of Controlled Release, 307: 16–31.
7. Joshi, N. C. and Prakash, Y. A. (2019). Leaves extract-based biogenic synthesis of cupric oxide nanoparticles, characterizations, and antimicrobial activity. Asian Journal of Pharmaceutical and Clinical Research, 12(8): 288-291.

8. Yaqoob, A. A.; Parveen, T.; Umar, K. and Mohamad Ibrahim, M. N. (2020). Role of nanomaterials in the treatment of wastewater: A review. Water, 12(2): 495.
9. Sharma, G.; Kumar, A.; Sharma, S.; Naushad, M.; Prakash Dwivedi, R.; ALOthman, Z.A., *et al*. (2019). Novel development of nanoparticles to bimetallic nanoparticles and their composites: A review. *Journal of King Saud University-Science,* 31: 257–269.
10. Belenov, S. V.; Volochaev, V. A.; Pryadchenko, V. V.; Srabionyan, V. V.; Shemet, D. B.; Tabachkova, N. Y., *et al*. (2017). Phase behavior of Pt–Cu nanoparticles with different architecture upon their thermal treatment. Nanotechnologies in Russia, 12: 147-155.
11. Suhail R. N., Mustafa S. A. & AL-Obodi E.E., Effciency of silver nanoparticles as antibacterial against Aeromonas Hydrophila isolated from infected Common Carp, Iraqi Journal of Agricultural Sciences –2022:53(3):589- 597.
12. World Health Organization (WHO) (2003). Basic laboratory procedures in clinical bacteriology. 2nd ed. *Genev*, Switzerland. Book.
13. Clinical and Laboratory Standards Institute (CLSI). (2023). Performance Standards for Antimicrobial Susceptiblity Testing 33rd ed. CLSI supplement M100 (ISBN 978-1-68440-170-3 IPrintl: ISBN 978-1-68440-171-0 Electronich), Clinical and Laboratory Standards Institute, USA.
14. Patel, F. M.; Goswami, P. N. and Khara, R. (2016). Detection of Biofilm formation in device associated clinical bacterial isolates in cancer patients. Sri Lankan Journal of Infectious Diseases, 6(1): 43-50.
15. Kirmusaoglu, S. (2019). The Methods for Detection of Biofilm and Screening Antibiofilm Activity of Agents. In Exopolysaccharides-Methods of Preparation and Application. *In technology Open.*
16. Ojha, S.; Sett, A. and Bora, U. (2017). Green synthesis of silver nanoparticles by *Ricinus communis* var. carmencita leaf extract and its antibacterial study. Advances in Natural Sciences: Nanoscience and Nanotechnology, 8(3): 35-39. Advances in Natural Sciences: Nanoscience and Nanotechnology.
17. Kadhim, R. M.; Al-Abodi, E. E. and Al-Alawy, A. F. (2018). Citrate-coated magnetite nanoparticles as osmotic agent in a forward osmosis process. Desalination and Water Treatment, 115: 45-52. Desalination and Water Treatment.
18. Jdayea.N. A, Al-Abodi E E.Biosynthesis of nanoparticles from plant extracts and their applications in medical treatments and drug delivery: Anbar Journal of Agricultural Sciences 2024, 22(2): 1240-1259. https://doi.org/10.32649/ajas.2024.184478
19. Iravani, S.; Korbekandi, H.; Mirmohammadi, S. V. and Zolfaghari, B. (2014). Synthesis of silver nanoparticles: chemical, physical and biological methods. *Research in pharmaceutical sciences*. 9(6): 385.
20. Dimitrijevic, R.; Cvetkovic, O.; Miodragović, Z; Simic, M; Manojlović, D. and Jovic, V. (2013). SEM/EDX and XRD characterization of silver nanocrystalline thin film prepared from organometallic solution precursor. Journal of Mining and Metallurgy B: Metallurgy, 49(1): 91-95.
21. Taher N. G. & E. E. AL- Abodi(2023) Anticancer activity of synthesized green silver nanoparticles against human colon cancer cell lines Oncology and Radiotherapy, 17 (11) 2023: 001-006 .
22. Ohikhena, F. U.; Wintola, O. A. and Afolayan, A. J. (2017). Evaluation of the Antibacterial and Antifungal Properties of *Phragmanthera capitata* (Sprengel) Balle (Loranthaceae), a Mistletoe Growing on Rubber Tree, Using the Dilution Techniques. *The Scientific World Journal*, Article ID 9658598. 8 pages.
23. SAS. (2012). Statistical Analysis System, User's Guide. Statistical. Version 9.1th ed. SAS. Inst. Inc. Cary. N.C. USA.
24. Saderi, H. and Owlia, P. (2015). Detection of multidrug resistant (MDR) and extremely drug resistant (XDR) *P. aeruginosa* isolated from patients in Tehran, Iran. Iranian journal of pathology, 10: 265.
25. Mahdi, L. F. and AL-Azawi, A. H. (2022). Synergistic Effect of Conocarpus erectus Extract and some Antibiotics against Multi-Drug Resistant Pseudomonas aeruginosa. Iraqi Journal of Biotechnology, 21(2): 308-325.
26. Fouad, H. Li. H. J. and Hosni, D. (2018). Controlling Aedes albopictus and Culex pipiens pallens using silver nanoparticles synthesized from aqueous extract of Cassia fistula fruit pulp and its mode of action. Artificial cells, nanomedicine, and biotechnology, 46(3): 558-567.

27. Saheed, Y.; Umar, A.F. and IIiyasu, M.Y. (2020). Potential of silver nano particles synthesized from *Ficus sycomorus* Linn against multidrug resistant Shigella species isolated from clinical specimens. American Journal of Life Sciences, 8(4): 82-90.
28. Pandey, A.; Sharma, S.K.; Singh, L. and Singh, T. (2013). An overview on Desmostachya bipinnata. Journal of Drug Discovery and Therapeutics, 7: 67–68.
29. Hadjiivanov, K.I.; Panayotov, D.A.; Mihaylov, M.Y.; Ivanova, E.Z.; Chakarova, K.K.; Andonova, S.M. *et al*. (2021). Power of infrared and raman spectroscopies to characterize metal organic frameworks and investigate their interaction with guest molecules. Chemical Review, 121: 1286-1424.
30. Singh, A.; Mittal, S.; Shrivastava, R.; Dass, S. and Srivastava, J.N. (2012). Biosynthesis of silver nanoparticles using *Ricinus communis* leaf extract and its antibacterial activity. Digest Journal of Nanomaterials and Biostructures, 7(3): 1157–1163.
31. Al-Khafaji, A. R. and Al-Azawi, A. H. (2022). Green Method Synthesis of Silver Nanoparticles Using Leaves Extracts of Rosmarinus officinalis. Iraqi Journal of Biotechnology, 21(2): 251-267.
32. Das, G.; Patra, J. K.; Nagaraj Basavegowda, C. N. V. and Shin, H. S. (2019). Comparative study on antidiabetic, cytotoxicity, antioxidant and antibacterial properties of biosynthesized silver nanoparticles using outer peels of two varieties of *Ipomoea batatas* (L.) Lam. International journal of nanomedicine. 14: 4741.
33. Jabbar Almukhtar, J. G. and Karam, F. F. (2020). Preparation characterization and application of Chitosan nanoparticles as drug carrier. Journal of Physics: Conference Series, 1664(1).
34. Pirtarighat, S.; Maryam, G. and Saeid, B. (2018). Green synthesis of silver nanoparticles using the plant extract of *Salvia spinosa* grown in vitro and their antibacterial activity assessment. Journal of Nanostructure in Chemistry, 9: 1-9.
35. Surega, R. (2015). Green synthesis of bioactive silver nanoparticles using plant extracts and their antinemic properties. PhD. Thesis, College of Agricalture, Tamil Nadu Agricultural University, Coimbatore.
36. Thamer, N. A. (2016). Green Synthesis of Silver Nanoparticles Using *Crocus Sativus* L. Extracts and Evaluation of some Biological Effects in Induced Pre-Hepatocellular Carcinoma in Male Rats. PhD Thesis, College of Science, University of Babylon, Iraq.
37. Rajoriya, I. P. (2017). Green synthesis of silver nanoparticles, their characterization and antimicrobial potential. PhD thesis, Jacob Institute of Biotechnology and Bioengineering, Sam Higginbottom University of Agriculture, Technology & Sciences, Allahabad, India.
38. Dakal, T. C.; Kumar, A.; Majumdar, R. S. and Yadav, V. (2016). Mechanistic basis of antimicrobial actions of silver nanoparticles, Frontiers in microbiology, 7: 1831.
39. Vega-Jiménez, A. L.; Vázquez-Olmos, A. R.; Acosta-Gío, E. and Álvarez-Pérez, M. A. (2019). In vitro antimicrobial activity evaluation of metal oxide nanoparticles. Nanoemulsions - Properties, Fabrications and Applications, 1-18.
40. Zhang, J.; Ma, J.; Fan, X.; Peng, W.; Zhang, G.; Zhang, F*., et al*. (2017). Graphene supported Au-Pd-Fe3O4 alloy trimetallic nanoparticles with peroxidase-like activities as mimic enzyme. Catalysis Communications, 89: 148-151.
41. Godfrey, I. J.; Dent, A. J.; Parkin, I. P.; Maenosono, S. and Sankar, G. (2017). Structure of gold–silver nanoparticles. The Journal of Physical Chemistry C, 121(3): 1957-1963.
42. Arora, N.; Thangavelu, K. and Karanikolos, G. N. (2020). Bimetallic nanoparticles for antimicrobial applications. Frontiers in Chemistry, 8: 412.
43. Basavegowda, N. and Baek, K. H. (2021). Multimetallic Nanoparticles as Alternative Antimicrobial Agents: Challenges and Perspectives. Molecules, 26(4): 912.
44. Guo, Z.; Chen, Y.; Wang, Y.; Jiang, H. and Wang, X. (2020). Advances and challenges in metallic nanomaterial synthesis and antibacterial applications. Journal of Materials Chemistry B, 8(22): 4764-4777.
45. Ogunyemi, S. O.; Zhang, F.; Abdallah, Y.; Zhang, M.; Wang, Y.; Sun, G*., et al*. (2019b). Biosynthesis and characterization of magnesium oxide and manganese dioxide nanoparticles using Matricaria chamomilla L. extract and its inhibitory effect on Acidovorax oryzae strain RS-2. Artificial cells, nanomedicine, and biotechnology, 47(1): 2230-2239.
46. Wang, L.; Hu, C. and Shao, L. (2017). The antimicrobial activity of nanoparticles: present situation and prospects for the future. International journal of nanomedicine, 12: 1227.

47. Azhir, E.; Etefagh, R.; Mashreghi, M. and Pordeli, P. (2015). Preparation, characterization and antibacterial activity of manganese oxide nanoparticles. Physical Chemistry Research, 3(3): 197-204.
48. Packirisamy, R. G.; Govindasamy, C.; Sanmugam, A.; Karuppasamy, K.; Kim, H. S. and Vikraman, D. (2019). Synthesis and antibacterial properties of novel ZnMn2O4–chitosan nanocomposites. Nanomaterials, 9(11): 1589.
49. Thibeaux, R.; Kainiu, M. and Goarant, C. (2020). Biofilm formation and quantification using the 96-microtiter plate. In Leptospira spp. Methods and Protocols (207-214). New York, NY: Springer US.
50. AL-Azawi, A. H. **(**2017). Phytochemical, Antibacterial and Antioxidant Activities of *dodonea viscosa* Jacq. extracts Cultivated. Iraqi Journal of Biotechnology, 16(4): 37-46.
51. Senobar Tahaei, S. A.; Stájer, A.; Barrak, I.; Ostorházi, E.; Szabó, D. and Gajdács, M. (2021). Correlation between biofilm-formation and the antibiotic resistant phenotype in *Staphylococcus aureus* isolates: a laboratory-based study in Hungary and a review of the literature. Infection and drug resistance, 1155-1168.
52. Ramos, G.; Rocha, J. and Tuon, F. (2013). Seasonal humidity may influence *Pseudomonas aeruginosa* hospital acquired infection rates. International Journal of Infectious Diseases. 17: 757-761.
53. Rajkumari, J.; Busi, S.; Vasu, A. C. and Reddy, P. (2017). Facile green synthesis of baicalein fabricated gold nanoparticles and their antibiofilm activity against *Pseudomonas aeruginosa* PAO1. Microbial pathogenesis, 107: 261-269.
54. Cai, L.; Chen, J.; Liu, Z.; Wang, H.; Yang, H. and Ding, W. (2018). Magnesium oxide nanoparticles: effective agricultural antibacterial agent against Ralstonia solanacearum. Frontiers in microbiology, 9: 790.
55. AL-Rubaye H. I. 1, B. k. AL-Rubaye1, E. E. Al-Abodi1a, E. I. Yousif " Green Chemistry Synthesis of Modified Silver Nanoparticles" Journal of Physics: Conference Series1664 (2020).012080IOPPublishingdoi:10.1088/1742-6596/1664/1/012080.